POLYOXOMETALATES REVIEW ARTICLE

Recent advances on the synthesis, structure, and properties of polyoxotantalates

Yuan Guan, Hui-Ping Xiao, Xin-Xiong Li✉, and Shou-Tian Zheng✉

Fujian Provincial Key Laboratory of Advanced Inorganic Oxygenated-Materials, College of Chemistry, Fuzhou University, Fuzhou 350108, China

Cite This: *Polyoxometalates*, **2023**, *2*, 9140023 Read Online

ABSTRACT: Polyoxotantalates (POTas) are an important branch of polyoxometalates (POMs) that remain largely undeveloped compared with other members of the POM family including polyoxovanadates, polyoxotungstates, polyoxomolybdates, and polyoxoniobates. Owing to their promising applications in diverse fields such as photo/electrocatalysis, ion conduction, environmental protection, and magnetism, the development of synthetic strategies for new POTas has attracted continuous interest over the past decades. This review summarizes the current status in the development of POTas, including their synthetic methods, crystal structures, physicochemical properties, and potential applications. Additionally, synthetic challenges and prospects are also discussed. It is hoped that this review will be of reference value for the further development of POTas.

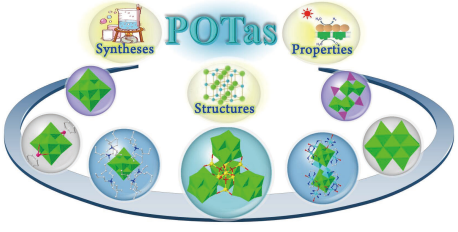

KEYWORDS: polyoxometalate, polyoxotantalate, ion conduction, photocatalysis

1 Introduction

Polyoxometalates (POMs), a unique class of inorganic metal oxide clusters constructed from corner-sharing and edge-sharing molybdenum/tungsten/vanadium/niobium/tantalum–oxygen polyhedra, have nearly 200 years of research history [1–8]. By virtue of their diverse structures, constituent elements and tunable molecular sizes, POMs have potential applications as functional materials in various fields such as industrial catalysis, environmental science, life science, and pharmacology [9–12]. Along with the advances in synthetic science and characterization technologies, POMs have witnessed a rapid development in recent years. However, among the POM family, the study of polyoxotantalates (POTas) still lags far behind that of polyoxomolybdates (POMos), polyoxotungstates (POTs), polyoxovanadates (POVs), and polyoxoniobates (PONbs) [13–20], and the number of POTas remains very limited so far since the first reported POTa in 1953 [21] owing mainly to the strong alkaline working environment, low solubility, and extraordinary inertness of tantalate species [22]. Nevertheless, the synthesis of new POTas has recently gained renewed interest from material researchers because POTas show promising applications in photocatalysis, base-catalyzed reactions, and as conducting materials. POTas usually exhibit a bandgap between the highest occupied molecular orbital and the lowest unoccupied molecular orbital comparable to that of Ta_2O_5 semiconductors, as well as high surface charge and basicity [23], which have prompted intense research efforts leading to some interesting discoveries.

Compared with the numerous critical reviews that have been published on the advances of POMos, POTs, POVs, and PONbs [24–28], reviews exclusively focusing on the development of POTas remain scarce [29]. Thus, a comprehensive review on the development of POTas, including their synthesis, structures, properties, and applications, will be of value to researchers in this area to promote further development of POTas. This review is divided into three parts. First, available synthetic strategies for POTas are summarized. Subsequently, advances in POTas are reviewed by separating known POTas into four subtypes according to their charge-balancing ions and skeleton configuration (Table 1). Finally, current challenges and prospects are presented.

2 Synthesis of POTas

The exploration of new POTas to enrich their structural diversity has been attracting continuous interest. However, due to the lanthanide contraction, tantalate species are too inert to form new cluster species [30]. Furthermore, the strong alkalinity of POTas hinders their reaction with various acidic transition metal ions.

Received: October 5, 2022; **Revised:** November 23, 2022
Accepted: December 25, 2022

✉Address correspondence to Xin-Xiong Li, lxx@fzu.edu.cn; Shou-Tian Zheng, stzheng@fzu.edu.cn

Table 1 A summary of reported POTAs[a]

Entry	Formula	Ta sources	Year published	Ref.
1	$K_8Ta_6O_{19}·17H_2O$	Ta_2O_5	1953	[21]
2	$K_7NaTa_6O_{19}·14H_2O$	Ta_2O_5	1997	[31]
3	$K_8Ta_6O_{19}·16H_2O$	Ta_2O_5	1997	[31]
4	$A_8[Ta_6O_{19}]·nH_2O$ (A = Rb, Cs; *n* = 0, 4, 14)	Ta_2O_5	2001	[32]
5	$Rb_6Na_2Ta_6O_{19}·23H_2O$	$TaCl_5$	2007	[19]
6	$Na_8Ta_6O_{19}·15H_2O$	$TaCl_5$	2007	[19]
7	$[Na_6(H_2O)_{13}]·[Li(H_2O)(H_3O)]·[Ta_6O_{19}]$	$K_8Ta_6O_{19}·17H_2O$	2009	[33]
8	$Li_8[Ta_6O_{19}]·24H_2O$	$Na_8Ta_6O_{19}·24.5H_2O$	2009	[22]
9	$Na_8Ta_6O_{19}·24.5H_2O$	Ta_2O_5	2011	[20]
10	$Na_8Ta_6O_{19}·26H_2O$	H_2TaF_7	2012	[34]
11	$TBA_6[H_2Ta_6O_{19}]$	$K_8Ta_6O_{19}·17H_2O$	2011	[35]
12	$TMA_4Ta_6O_{17}$	$Ta(OC_2H_5)_5$	2012	[36]
13	$TBA_{3.5}[H_{4.5}(Ta_6O_{19})]·2THF·5.5H_2O$	$Ta_2O_5·nH_2O$	2012	[37]
14	$TBA_6[Ta_{10}O_{28}]·6H_2O$	$TBA_6[H_2Ta_6O_{19}]$	2013	[38]
15	$K_7[Re(CO)_3Ta_6O_{19}]$	$K_8Ta_6O_{19}·17H_2O$	2001	[39]
16	$K_7[Mn(CO)_3Ta_6O_{19}]$	$K_8Ta_6O_{19}·17H_2O$	2001	[39]
17	*cis*-$K_6[\{Mn(CO)_3\}_2Ta_6O_{19}]$	$K_8Ta_6O_{19}·17H_2O$	2001	[39]
18	*trans*-$K_4Na_2[\{Re(CO)_3\}_2Ta_6O_{19}]$	$K_8Ta_6O_{19}·17H_2O$	2001	[39]
19	$[Cu(1,3\text{-dap})_2]_2[Cu(1,3\text{-dap})(H_2O)]_2[Ta_6O_{19}]·8H_2O$	$K_8Ta_6O_{19}·17H_2O$	2011	[40]
20	$[Cu(en)_2]_4[Ta_6O_{19}]·14H_2O$	$K_8Ta_6O_{19}·17H_2O$	2011	[40]
21	Na_4(*trans*-$[\{(C_6H_6)Ru\}_2Ta_6O_{19}]·20H_2O$	$Na_8Ta_6O_{19}·24.5H_2O$	2014	[41]
22	$Cs_4[(Cp^*Rh)_2Ta_6O_{19}]·18H_2O$	$Cs_8[Ta_6O_{19}]·14H_2O$	2014	[42]
23	$Na_6[\{Cp^*Ir\}Ta_6O_{19}]·27H_2O$ (Na_6-$IrTa_6$)	$Na_8Ta_6O_{19}·24.5H_2O$	2016	[43]
24	Na_4[*trans*-$\{Cp^*Ir\}_2Ta_6O_{19}]·24H_2O$	$Na_8Ta_6O_{19}·24.5H_2O$	2016	[43]
25	$Na_4(NH_4)_2[(Ta_6O_{19})Co(H_2O)_3]·20H_2O$	$K_8Ta_6O_{19}·17H_2O$	2019	[44]
26	$\{[CuL^1]_2[CuL^1_2]_2[Ta_6O_{19}]\}·21H_2O$	$K_8Ta_6O_{19}·17H_2O$	2019	[45]
27	$\{[CuL^2]_2[CuL^2_2]_2[Ta_6O_{19}]\}·20H_2O$	$K_8Ta_6O_{19}·17H_2O$	2019	[45]
28	$Na_{10}[\{(C_6H_6)RuTa_6O_{18}\}_2(\mu\text{-}O)]·39.4H_2O$	$Na_8Ta_6O_{19}·24.5H_2O$	2014	[41]
29	$Na_4K_6[(Ta_6O_{19})Co(en)]_2·30H_2O$	$K_8Ta_6O_{19}·17H_2O$	2019	[44]
30	$K_2[Ni(dien)_2]\{[Ni(dien)]_2Ta_6O_{19}\}·11H_2O$	$K_8Ta_6O_{19}·17H_2O$	2021	[46]
31	$K_4\{[Cu(cyclam)]_2Ta_6O_{19}\}·18H_2O$	$K_8Ta_6O_{19}·17H_2O$	2021	[47]
32	$K_4\{[Zn(cyclam)]_2Ta_6O_{19}\}·18H_2O$	$K_8Ta_6O_{19}·17H_2O$	2021	[47]
33	$\{[Cd(cyclam)]_4Ta_6O_{19}\}·19H_2O$	$K_8Ta_6O_{19}·17H_2O$	2021	[47]
34	$H_2[Cu(en)_2(H_2O)_2]\{[Cu(en)_2]_4[Cu(en)(Ta_6O_{19})]_2\}·14H_2O$	$Na_8Ta_6O_{19}·24.5H_2O$	2019	[48]
35	$H_2\{[Cu(en)_2]_3[Cu(en)(H_2O)_2Cu(en)(Ta_6O_{19})]_2\}·30H_2O$	$Na_8Ta_6O_{19}·24.5H_2O$	2019	[48]
36	$H_2[Cu(enMe)_2(H_2O)_2][Na_2(H_2O)_{10}]_2\{[Cu(enMe)_2]_2[Cu(enMe)(Ta_6O_{19})]_2\}·26H_2O$	$Na_8Ta_6O_{19}·24.5H_2O$	2019	[48]
37	$H_4[Na_4(H_2O)_{18}]\{[Cu(enMe)_2]_2[Cu(enMe)(Ta_6O_{19})]_2\}·10H_2O$	$Na_8Ta_6O_{19}·24.5H_2O$	2019	[48]
38	$H_2[Cu(en)_2(H_2O)_2]\{[Cu(en)_2]_2[Na_2(H_2O)_7]_2[Cu(en)(Ta_6O_{19})]_2\}·10H_2O$	$Na_8Ta_6O_{19}·24.5H_2O$	2019	[48]
39	$H_2[Na_2(H_2O)_{10}]_2[Cu(en)_2]_2\{[Cu(en)_2][Cu(en)(Ta_6O_{19})]_2\}·8H_2O$	$Na_8Ta_6O_{19}·24.5H_2O$	2019	[48]
40	$TMA_8Ti_2Ta_8O_{28}·21H_2O$	$Ta_2O_5·nH_2O$	2016	[49]
41	$TMA_{10}Ti_{12}Ta_6O_{44}·39H_2O$	$Ta_2O_5·nH_2O$	2016	[49]
42	$Cs_3[H_9P_4Ta_6(O_2)_6O_{25}]·9H_2O$	$K_8Ta_6O_{19}·17H_2O$	2017	[50]
43	$(CN_3H_6)_6[H_4P_4Ta_6(O_2)_6O_{24}]·4H_2O$	$K_8Ta_6O_{19}·17H_2O$	2017	[50]
44	$Na_8K_7[H_5Co_8Ta_{24}O_{80}]·45H_2O$	$K_8Ta_6O_{19}·17H_2O$	2018	[51]
45	$Cs_3[Ln^1(H_2O)_6\{H_4(TaO_2)_6As_4O_{24}\}]·7H_2O$	$K_8Ta_6O_{19}·17H_2O$	2019	[52]
46	$KNa_2[HSe_2(TaO_2)_6(OH)_4(H_2O)_2O_{13}]·15H_2O$	$K_8Ta_6O_{19}·17H_2O$	2021	[53]
47	$Cs_2K_{1.5}Na_{1.5}[Se_4(TaO_2)_6(OH)_3O_{18}]·17H_2O$	$K_8Ta_6O_{19}·17H_2O$	2021	[53]
48	$Cs_3H_3[Ni_2(H_2O)_4\{P_4Ta_6(O_2)_6O_{24}\}]·7H_2O$	$K_8Ta_6O_{19}·17H_2O$	2022	[54]
49	$Cs_3NaH_4[Zn(H_2O)_4\{P_4Ta_6(O_2)_6O_{24}\}]·13H_2O$	$K_8Ta_6O_{19}·17H_2O$	2022	[54]
50	$Cs_3NaH_4[Cd(H_2O)_4\{P_4Ta_6(O_2)_6O_{24}\}]·8H_2O$	$K_8Ta_6O_{19}·17H_2O$	2022	[54]
51	$CsK[Ln^2(H_2O)_6Se_4(TaO_2)_6(OH)_3O_{18}]·nH_2O$	$K_8Ta_6O_{19}·17H_2O$	2022	[55]

[a]TBA = tetra-*n*-butylammonium, THF = tetrahydrofuran, en = ethylenediamine, 1,3-dap = 1,3-diaminopropane, L^1 = 1,10-phen, L^2 = 2,2'-bipy, Cp* = pentamethylcyclopentadienyl, dien = diethylenetriamine, cyclam = 1,4,8,11-tetraazacyclotetradecane, enMe = 1,2-diaminopropane, Ln^1 = Sm, Eu, Tb, Dy, Er, Tm, Yb, Lu, Ln^2 = Eu, Gd, Lu.

Therefore, the synthesis of new POTas is a challenging task. Nevertheless, the efforts of POM chemists and the rapid development of modern synthetic techniques have provided new examples in recent years. At present, there are four main synthetic strategies for POTas: (1) solid-state reactions between Ta_2O_5 and different alkaline hydroxides at high temperature, which often results in the formation of a variety of alkaline metal charge-balanced $[Ta_6O_{19}]^{8-}$ (**Ta_6**); (2) hydrothermal/solvothermal reactions using alkaline metal charge-balanced Ta_6 species as precursors, which have led to some new POTas and organic salts of **Ta_6**; (3) slow evaporation or diffusion with poor solvents of the filtrate of hydrothermal/solvothermal reactions for crystallization, which can be regarded as a post-treatment of the second strategy; (4) conventional solution/water-bath reactions of **Ta_6** with various transition metal ions and organic ligands in the presence of hydrogen peroxide followed by slow crystallization. Among the above strategies, using alkaline metal charge-balanced **Ta_6** as precursors is the most widely applied. In addition, organic salts of **Ta_6** can serve as precursors to generate new POTas via solvothermal reactions. However, the exploration of POTas based on organic **Ta_6** precursors is still limited probably because of the inconvenience of the large-scale preparation of organic salts of **Ta_6**.

3 POTas and their properties

It is a common perception that tantalum is chemically similar to niobium on account of the lanthanide contraction. Owing to their similar electronic configurations, their pentavalent ions and polyoxoanions are nearly identical in size. This remarkable discovery paved the way for the exploration of POTas. Lindqvist-type **Ta_6** (Fig. 1) is a large octahedron composed of six TaO_6 octahedrons sharing edges and exhibits approximate O_h spatial symmetry. The oxygen atoms of **Ta_6** can be classified into three types according to their bonding modes: i) six terminal oxygen atoms (O_t), ii) twelve bridging oxygen atoms (O_b), and iii) one six-coordinate central oxygen atom (O_c). Therefore, the Ta–O bond length lies within the ranges 1.780–1.805, 1.972–2.008, and 2.368–2.378 Å for Ta–O_t, Ta–O_b, and Ta–O_c, respectively. The O–Ta–O bond angles are in the range of 77.14°–178.44° [56].

3.1 Inorganic POTas based on Ta_6 polyanion and alkali metal anions

The first POTa was reported by Lindqvist in 1953; accordingly, it was named Lindqvist-type $K_8Ta_6O_{19}{\cdot}17H_2O$ [21]. Subsequently, POTas having the general formula $M_8Ta_6O_{19}$ (M = K, Na, Li, Cs) were successively reported [17, 32]. In 1997, the first POTa containing two different alkali metals as countercations, $K_7NaTa_6O_{19}{\cdot}14H_2O$, was reported by Berlin [17]. In 2001, a POTa containing different lattice water molecules was reported, namely

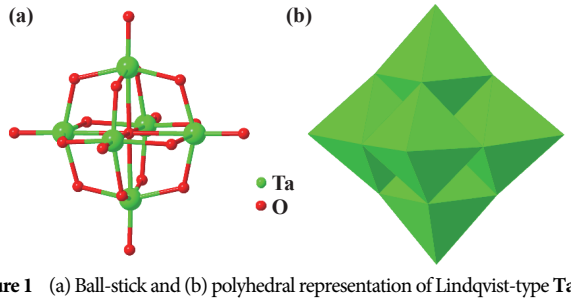

Figure 1 (a) Ball-stick and (b) polyhedral representation of Lindqvist-type **Ta_6**.

$A_8[Ta_6O_{19}]{\cdot}nH_2O$ (A = Rb, Cs; n = 0, 4, 14) [32]. Since then, other POTas constructed with different alkali metal ions as countercations have been reported, including $Rb_6Na_2Ta_6O_{19}{\cdot}23H_2O$, $Na_8Ta_6O_{19}{\cdot}15H_2O$, and $Li_8[Ta_6O_{19}]{\cdot}24H_2O$ [19]. In 2009, Hu et al. successfully synthesized $[Na_6(H_2O)_{13}]{\cdot}[Li(H_2O)(H_3O)]{\cdot}[Ta_6O_{19}]$, the first three-dimensional (3D) POTa with $[Na_6(H_2O)_{13}]^{6+}$ and $[Li(H_2O)]^{+}$ as countercations [33], in which **Ta_6** is surrounded by Na^+ and Li^+ ions. The Na^+ ion is octahedrally bonded by six O atoms. Li^+ ions are linked by four O atoms (two O atoms from two **Ta_6** anions and two O atoms from four water molecules). $[Na_6(H_2O)_{13}]^{6+}$ hexamers are composed of two $[Na_3(H_2O)_{13}]^{3+}$ trimers in different directions. The $[Na_3(H_2O)_{13}]^{3+}$ trimers are formed by three edge-sharing NaO_6 octahedra. The Na atom binds to the **Ta_6** anion by an O_t. Therefore, the $[Na_6(H_2O)_{13}]^{6+}$ hexamers serve as bridges linking the **Ta_6** units to a one-dimensional (1D) ladder chain. Then, through Li–O linkages, the 1D ladder chains form two-dimensional (2D) layers, which are further interconnected through Na–O linkages to form a 3D framework (Fig. 2). **Ta_6** has been demonstrated to exhibit photocatalytic activity, effectively degrading methylene blue in water under UV light irradiation. The degradation efficiency depends on experimental conditions such as pH, irradiation time, and the initial concentration of methylene blue.

Subsequently, Abramov simplified and refined the preparation process of $Na_8Ta_6O_{19}{\cdot}24.5H_2O$ in 2011, greatly improving the yield and providing a prerequisite for the use of $Na_8Ta_6O_{19}{\cdot}24.5H_2O$ as a precursor [20]. The use of alkali metals as countercations in the synthesis of POTas is relatively mature, and the yields of some alkali metal-containing POTas (K, Na) have been greatly improved. Although no POTas having a configuration other than the Lindqvist configuration have been reported, great progress has been made by introducing different metals and heteroatoms.

3.2 Inorganic–organic hybrid POTas based on Ta_6 polyanion and organic cations

Owing to their complicated preparation process, inorganic–organic hybrid POTas, in which an organic cation counteracts with **Ta_6**, are scarce. In 2011, Yagasaki et al. synthesized and structurally characterized $TBA_6[H_2Ta_6O_{19}]$ [35], which is the first organic salt of POTas and the first protonated Lindqvist-type Ta_6. This compound was synthesized and isolated as a tetra-*n*-butylammonium (TBA) salt by treating $K_8[Ta_6O_{19}]$ with HCl to produce hydrous tantalum oxide (symbolically written as $H_8[Ta_6O_{19}]$), followed by dissolving the oxide with TBAOH in water. $TBA_6[H_2Ta_6O_{19}]$ can be recrystallized from toluene/Et_2O. In Yagasaki's work, the locations of the protons were inferred by comparing the bond lengths and calculating the bond valence. Considering that the O_b atoms of **Ta_6** are more basic and reactive than the O_t atoms, the former are most likely the protonation sites. Since the lack of protonated precursors has hampered the development of POTas, the discovery of $TBA_6[H_2Ta_6O_{19}]$ is likely to pave the way for the synthesis of high-nuclearity POTas (Fig. 3(c)).

$TMA_4Ta_6O_{17}{\cdot}nH_2O$ was found in 2012 by Ohya [36]. Meanwhile, Yagasaki et al. reported a POTa cluster, i.e., $TBA_{3.5}[H_{4.5}(Ta_6O_{19})]{\cdot}2THF{\cdot}5.5H_2O$, which is a hexatantalate tetramer held together by hydrogen bonds with solvent molecules floating around [37]. The $[H_{4.5}(Ta_6O_{19})]^{3.5-}$ anion forms a discrete, linear tetramer; therefore, $[H_{18}(Ta_6O_{19})_4]^{14-}$ would be a more appropriate formulation. In the anion, four **Ta_6** units are linked by 18 hydrogen bonds to form a nearly 30 Å-long rod-like

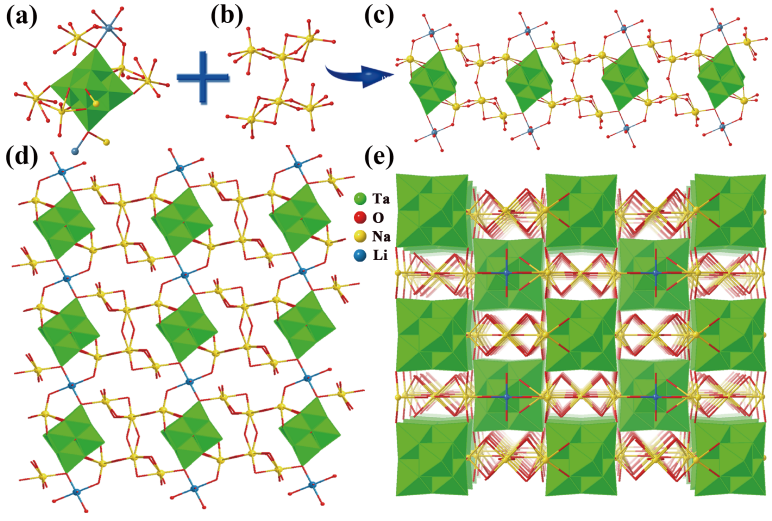

Figure 2 (a)–(c) Ball-and-stick diagram of the polyhedron formed by the interaction with Na, Li-containing $[Ta_6O_{19}]^{8-}$ with $[Na_6(H_2O)_{13}]^{6+}$ hexamers, and 1D ladder chain formed along the *a*-axis of $[Na_6(H_2O)_{13}][Li(H_2O)(H_3O)][Ta_6O_{19}]$. (d) View along the *c*-axis illustrating the infinite 2D layered structure of $[Na_6(H_2O)_{13}][Li(H_2O)(H_3O)]\cdot[Ta_6O_{19}]$. H atoms are omitted for clarity. (e) View of the 3D extended framework in $[Na_6(H_2O)_{13}][Li(H_2O)(H_3O)]\cdot[Ta_6O_{19}]$. H atoms are omitted for clarity. Polyhedral codes: TaO_6, green.

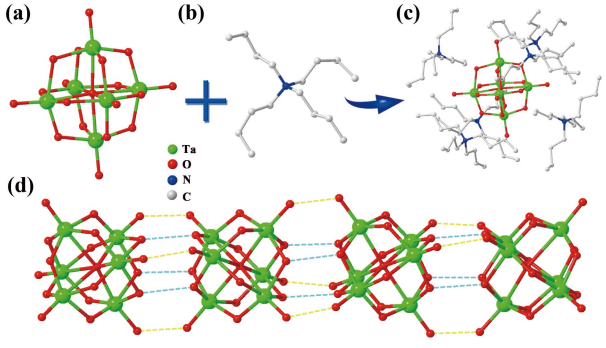

Figure 3 (a) Lindqvist-type $\mathbf{Ta_6}$. (b) Tetra-*n*-butylammonium (TBA). (c) Lindqvist-type Ta_6 counterbalanced by TBA. (d) The tetrameric anion cluster $[H_{18}(Ta_6O_{19})_4]^{14-}$ is linked together by hydrogen bonding. The strength of hydrogen bonds is indicated by different colors.

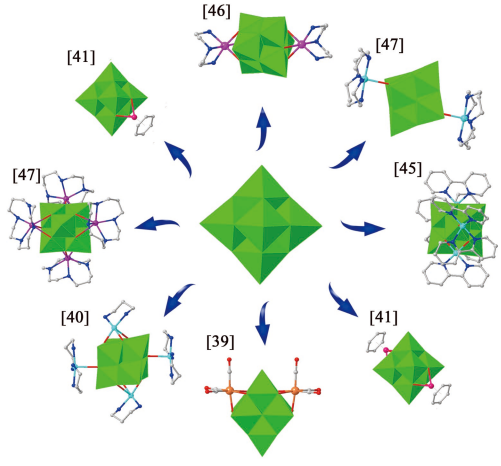

Figure 4 A summary of inorganic–organic hybrid POTas based on $\mathbf{Ta_6}$ and different metal complexes. Polyhedral codes: TaO_6, green.

supramolecule. Among the 18 hydrogen bonds, nine are moderately strong with O···O distances in the range of 2.69–2.74 Å (blue bonds in Fig. 3(d)), and the other nine are stronger hydrogen bonds with O···O distances in the range of 2.43–2.53 Å (yellow bonds in Fig. 3(d)). The former type of hydrogen bonds link doubly O_b atoms and the latter connect the O_t atoms of $\mathbf{Ta_6}$ units. The rod-like tetramer is formed by connecting four $\mathbf{Ta_6}$ units to each other in a face-to-face manner through 18 hydrogen bonds (Fig. 3(d)). The triangular faces of adjacent $\mathbf{Ta_6}$ units are aligned in the same direction.

3.3 Inorganic–organic hybrid POTas based on Ta_6 polyanion and metal complexes

The first organic–inorganic hybrid POTa, namely Ta_6–$K_7[\{M(CO)_3\}_nTa_6O_{19}]$ (M = Re, Mn, *n* = 1, 2), was reported in 2001 (Fig. 5) [39]. It is interesting to note that when *n* = 2 and M = Mn, the crystal is in *cis*-form (*cis*-$[Ta_6O_{19}\{Mn(CO)_3\}_2]^{6-}$), and when *n* = 2 and M = Re, the crystal adopts the *trans*-form (*trans*-$[Ta_6O_{19}\{Re(CO)_3\}_2]^{6-}$). The reaction of $[Re(CO)_3(CH_3CN)_3]ClO_4$ and $K_8[Ta_6O_{19}]$ must take place under inert gas protection. Additionally, $[Ta_6O_{19}\{Re(CO)_3\}_2]^{6-}$ has a broader pH tolerance

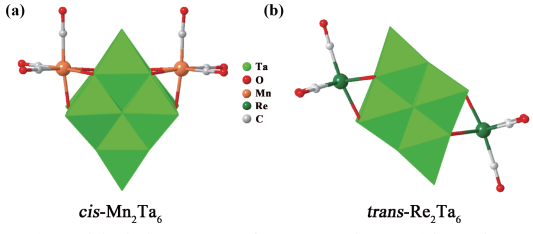

Figure 5 (a) Polyhedral structure of *cis*-$[Ta_6O_{19}\{Mn(CO)_3\}_2]^{6-}$. (b) Polyhedral structure of *trans*-$[Ta_6O_{19}\{Re(CO)_3\}_2]^{6-}$. Polyhedral codes: TaO_6, green.

range than $K_8[Ta_6O_{19}]$.

In 2009, Hu et al. synthesized the first 3D alkali metal-resistant POTa, and their intense efforts toward the development of POTas led to the successful introduction of Cu into $\mathbf{Ta_6}$. Specifically, they synthesized two POTa derivatives, i.e., $\{[Cu(1,3\text{-dap})_2]_2[Cu(1,3\text{-dap})(H_2O)]_2[Ta_6O_{19}]\}\cdot 8H_2O$ and $[Cu(en)_2]_4[Ta_6O_{19}]\cdot 14H_2O$ (1,3-dap = 1,3-diaminopropane; en = ethylenediamine), which were constructed from the Lindqvist-type $\mathbf{Ta_6}$ polyanion and Cu–amine complexes [40]. The $\mathbf{Ta_6}$ anion of $\{[Cu(1,3\text{-dap})_2]_2[Cu(1,3\text{-}$

dap)$(H_2O)]_2[Ta_6O_{19}]\}\cdot 8H_2O$ is attached to four Cu fragments via O_b to form a neutral cluster, which is then hydrogen-bonded through trimeric water to produce a 1D supramolecular chain. The **Ta_6** polyoxoanions of $[Cu(en)_2]_4[Ta_6O_{19}]\cdot 14H_2O$ are linked together by hydrogen bonds and weak interactions with Cu–O to form infinite 1D supramolecular chains, which are further linked by hydrogen bonds to cyclic water tetramers to produce a 2D supramolecular network (Fig. 6). Unlike the usual syntheses, CuI containing Cu^+ instead of Cu^{2+} was used. However, the oxidation state of the Cu ion was determined to be +2 via X-ray photoelectron spectroscopy and valence bond calculations. It is worth mentioning that the diffusion strategy was used in the crystallization process because slow evaporation was ineffective. The first example of Cu-incorporated POTas reported by Hu laid the foundation for the development of transition metal–containing POTas.

POMs can be regarded as polydentate oxygen-containing ligands that can combine with heterometals. To this aim, noble metals are particularly attractive because of their wide variety of oxidation states, which range from negative to highly positive (VIII for Ru and Os) [57, 58]. They can catalyze many chemical transformations, including water splitting [59–61]. Moreover, POMs can coordinate with organometallic fragments such as $\{(p\text{-cym})Ru\}^{2+}$ (*p*-cym = *p*-cymene) or $\{Cp^*Rh\}^{2+}$ (Cp* = pentamethylcyclopentadienyl), providing an attractive platform for the synthesis of hybrid complexes. Despite the intriguing properties of POMs and noble metals, few attempts have been made to coordinate noble metals with PONbs and POTas. In general, $\{Cp^*Rh\}^{2+}$ is an excellent building block for grafting on POMs because it possesses predictable coordination geometry and can be grafted on pre-existent POM species without changing their structure and for the coordination-induced formation of new POM frameworks.

Abramov et al. isolated simultaneously two new hybrid organometallic POTas by reacting $[(C_6H_6)RuCl_2]_2$ and $Na_8[Ta_6O_{19}]$. In this synthesis process, the coordination of $\{(C_6H_6)Ru\}^{2+}$ with **Ta_6** neutralizes the high negative charge of the precursor and reduces its protonation in aqueous solution, leading to the formation of the POTa. Using different POM/Ru ratios, single-capped $[(C_6H_6)RuTa_6O_{19}]^{6-}$ and doubly substituted $[\{(C_6H_6)Ru\}_2Ta_6O_{19}]^{4-}$ were obtained (Fig. 7). These authors also prepared single-capped $[\{Cp^*M\}Ta_6O_{19}]$ and double-capped *trans*-$[\{Cp^*M\}_2Ta_6O_{19}]^{4-}$ complexes (M = Rh, Ir) via the reaction of $\{Cp^*M\}$ (M = Rh, Ir) with **Ta_6** [41–43]. The choice of the appropriate reaction conditions for the synthesis of POTas $\{Cp^*M\}^{2+}$ is vital.

In 2019, Zhai et al. reported a new POTa cluster, i.e., $[(Ta_6O_{19})Co(H_2O)_3]^{6-}$, as the first example of **Ta_6** loaded with one Co ion [44]. In the same year, Niu et al. presented $\{[CuL]_2[CuL_2]_2[Ta_6O_{19}]\}\cdot 21H_2O$ (L = 1,10-phen) and $\{[CuL]_2[CuL_2]_2[Ta_6O_{19}]\}\cdot 20H_2O$ (L = 2,2'-bipy), which comprise a Lindqvist-type **Ta_6** acting as an octadentate ligand to coordinate two [CuL] units and two $[CuL_2]$ fragments through six O_b and two O_t atoms [45].

In 2021, Bensch et al. obtained crystals of $K_4\{[Cu(cyclam)]_2Ta_6O_{19}\}\cdot 18H_2O$, $K_4\{[Zn(cyclam)]_2Ta_6O_{19}\}\cdot 18H_2O$, and $\{[Cd\text{-}(cyclam)]_4Ta_6O_{19}\}\cdot 19H_2O$ by subjecting a mixture of $K_8\{Ta_6O_{19}\}\cdot 16H_2O$, d-block metal (M) salts (M = Cu, Zn, or Cd), and the macrocyclic ligand 1,4,8,11-tetraazacyclotetradecane (cyclam) to diffusion at room temperature [46, 47]. Cyclam was able to stabilize Lindqvist-type **Ta_6**, thus promoting the formation of novel POTas. In the isostructural compounds $K_4\{[Cu(cyclam)]_2Ta_6O_{19}\}\cdot 18H_2O$ and $K_4\{[Zn(cyclam)]_2Ta_6O_{19}\}\cdot 18H_2O$, the transition metals are attached to the anion cluster via Cu–O–Ta and Zn–O–Ta bonds, respectively. However, the geometry of the M^{2+} complexes is different, namely, Cu^{2+} exhibits a square cone geometry and Zn^{2+} a triangular bipyramidal geometry. In the structure of $\{[Cd(cyclam)]_4Ta_6O_{19}\}\cdot 19H_2O$, the Cd^{2+} cation shows a rare seven-coordinated single-ended triangular prismatic geometry and is covalently linked to the anion nucleus by a Cd–O–Ta bond. Bensch's team also prepared $K_2[Ni(dien)_2]\{[Ni(dien)]_2Ta_6O_{19}\}\cdot 11H_2O$ (dien = diethylenetriamine), in which **Ta_6** unfolded in a Ni^{2+} octahedron through three Ni–μ_2–O–Ta bonds, thus forming a new $\{[Ni(dien)]_2Ta_6O_{19}\}^{4-}$ anion [46]. With these successful attempts, Ni, Cd, and Zn elements were introduced into **Ta_6** for the first time.

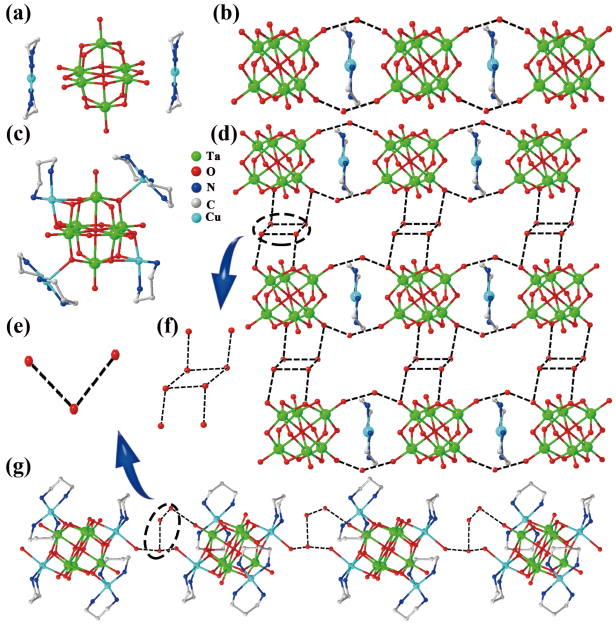

Figure 6 (a) Ball-and-stick representations of $[Cu(en)_2]_4[Ta_6O_{19}]\cdot 14H_2O$. (b) View of the 1D chain along the *a*-axis formed by hydrogen bonding between water molecules and the $[Ta_6O_{19}]^{8-}$ anions of $[Cu(en)_2]_4[Ta_6O_{19}]\cdot 14H_2O$. (c) Ball-and-stick representations of $\{[Cu(1,3\text{-dap})_2]_2[Cu(1,3\text{-dap})(H_2O)]_2[Ta_6O_{19}]\}\cdot 8H_2O$. (d) and (f) 2D framework of $[Cu(en)_2]_4[Ta_6O_{19}]\cdot 14H_2O$ constructed from 1D chains linked by $(H_2O)_4$ clusters via hydrogen bonding viewed along the *c*-axis direction and the cyclic water tetramer. (e) and (g) 1D framework of $\{[Cu(1,3\text{-dap})_2]_2[Cu(1,3\text{-dap})(H_2O)]_2[Ta_6O_{19}]\}\cdot 8H_2O$ linked by $(H_2O)_4$ clusters via hydrogen bonding viewed along the *a*-axis direction and water trimers.

3.4 High-nuclearity POTas derived from Ta_6 units

The previous sections have outlined different alkali metals and organic and inorganic hybrid complexes as countercations for **Ta_6**. Here, in addition to POTas existing in the form of **Ta_6**, other POTas derived from **Ta_6** will be discussed.

For instance, $Na_{10}[\{(C_6H_6)RuTa_6O_{18}\}_2(\mu\text{-O})]\cdot 39.4H_2O$ is a dimer of **Ta_6** formed during an intermediate reaction without breaking the Lindqvist configuration [41]. The formation of $[\{(C_6H_6)RuTa_6O_{18}\}_2(\mu\text{-O})]^{10-}$ can be regarded as a coordination-induced condensation of two **Ta_6** as follows:

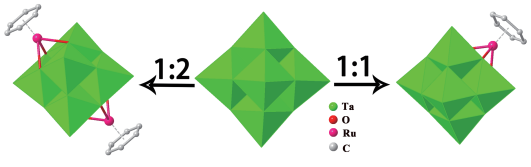

Figure 7 $[Ta_6O_{19}]^{8-}$ forms 1:1 and 1:2 complexes with $[(C_6H_6)RuCl_2]_2$. Polyhedral codes: TaO_6, green.

$$[\{(C_6H_6)Ru\}Ta_6O_{19}]^{6-} + H_2O = [\{(C_6H_6)Ru\}Ta_6O_{19}H]^{5-} + OH^-$$

$$2[\{(C_6H_6)Ru\}Ta_6O_{19}H]^{5-} = [\{(C_6H_6)RuTa_6O_{18}\}_2(\mu\text{-}O)]^{10-} + H_2O$$

The $[(Ta_6O_{19})Co(en)]_2^{10-}$ cluster is also a dimer of the $[(Ta_6O_{19})Co(H_2O)_3]^{6-}$ cluster, in which the water ligand is replaced by en. In 2019, Zheng et al. reported a series of novel inorganic-organic hybrid high-dimensional POTa materials, i.e., $H_2[Cu(en)_2(H_2O)_2]\{[Cu(en)_2]_4[Cu(en)(Ta_6O_{19})]_2\}\cdot 14H_2O$, $H_4[Na_4(H_2O)_{18}]\{[Cu(enMe)_2]_2[Cu(enMe)(Ta_6O_{19})]_2\}\cdot 10H_2O$, and other six substances (enMe = 1,2-diaminopropane) [48]. As far as we know, $H_2[Cu(en)_2(H_2O)_2]\{[Cu(en)_2]_4[Cu(en)(Ta_6O_{19})]_2\}\cdot 14H_2O$ and $H_2\{[Cu(en)_2]_3[Cu(en)(H_2O)_2Cu(en)(Ta_6O_{19})]_2\}\cdot 30H_2O$ are 3D POTas, whereas $H_2[Cu(enMe)_2(H_2O)_2][Na_2(H_2O)_{10}]_2\{[Cu(enMe)_2]_2[Cu(enMe)(Ta_6O_{19})]_2\}\cdot 26H_2O$ and $H_4[Na_4(H_2O)_{18}]\{[Cu(enMe)_2]_2[Cu(enMe)(Ta_6O_{19})]_2\}\cdot 10H_2O$ are 2D POTas. More interestingly, $H_2[Cu(en)_2(H_2O)_2]\{[Cu(en)_2]_4[Cu(en)(Ta_6O_{19})]_2\}\cdot 14H_2O$ and $H_2[Cu(enMe)_2(H_2O)_2][Na_2(H_2O)_{10}]_2\{[Cu(enMe)_2]_2[Cu(enMe)(Ta_6O_{19})]_2\}\cdot 26H_2O$ can undergo a single-crystal to single-crystal structural transition upon immersion in water. $H_2[Cu(en)_2(H_2O)_2]\{[Cu(en)_2]_4[Cu(en)(Ta_6O_{19})]_2\}\cdot 14H_2O$ crystallizes in the monoclinic space group $P2_1/c$, and its asymmetric unit consists of half a $\{CuTa_6\}_2$ secondary building unit (SBU), two $[Cu(en)_2]^{2+}$ complexes, and half a $[Cu(en)_2(H_2O)]^{2+}$ cation. $\{CuTa_6\}_2$ is composed of two centrosymmetric monocopper-capped Lindqvist-type POTa clusters, in which the octahedral Cu ion is captured by one $\{Ta_3O_3\}$ group of a $\{Ta_6O_{19}\}$ cluster through three O_b atoms. The rest of the coordination sites of the Cu ion are occupied by two N donors from one chelating en ligand and one O_t atom from a neighboring $\{Ta_6O_{19}\}$ cluster. In $H_2[Cu(en)_2(H_2O)_2]\{[Cu(en)_2]_4[Cu(en)(Ta_6O_{19})]_2\}\cdot 14H_2O$, each $\{CuTa_6\}_2$ cluster is surrounded by eight $[Cu(en)_2]^{2+}$ complexes (four Cu1 and four Cu3 complexes) to bind six neighboring $\{CuTa_6\}_2$ clusters. The $\{CuTa_6\}_2$ SBUs are first bridged by Cu3 complexes to form a 2D layer, and the neighboring symmetry-related layers are further integrated by Cu1 complexes, resulting in the formation of a 3D anionic framework (Fig. 8). This framework possesses large irregular 1D channels along the *a*-axis, which are filled with dissociative $[Cu(en)_2(H_2O)_2]^{2+}$ cations and lattice water molecules. From a topological point of view, the $\{CuTa_6\}_2$ SBUs can be regarded as six-connected nodes, and the whole framework can be simplified as a *pcu*-type topology. $H_2[Cu(en)_2(H_2O)_2]\{[Cu(en)_2]_4[Cu(en)(Ta_6O_{19})]_2\}\cdot 14H_2O$ was obtained in high yield and showed high stability; therefore, it was tested for proton conduction, finding that the conductivity increased significantly up to the highest value of 1.04×10^{-2} S·cm^{-1} upon increasing the temperature from 35 to 75°C at 98% relative humidity. This behavior could be attributed to the fact that the temperature increase accelerated the movement of water molecules in the channel (Fig. 9).

In 2018, the first Co-containing POTa cluster, $Na_8K_7H_5Co_8Ta_{24}O_{80}\cdot 45H_2O$, was obtained by Niu. This compound, which was the first example of a tetrameric type in the form of **Ta$_6$**, can be seen as a tetrahedral structure formed by four $\{Ta_6Co\}$ building blocks connected by four Co^{2+} ions. The Co ions in each $\{Ta_6Co\}$ unit are connected by O atoms to form an interesting $\{Co_4O_4\}$ cubane structure. The cubane holds four outer Co^{2+} ions through four μ_4-oxo bridges, while each Co^{2+} ion is bound to three O atoms of three neighboring $\{Ta_6Co\}$ units (Fig. 10). It should be

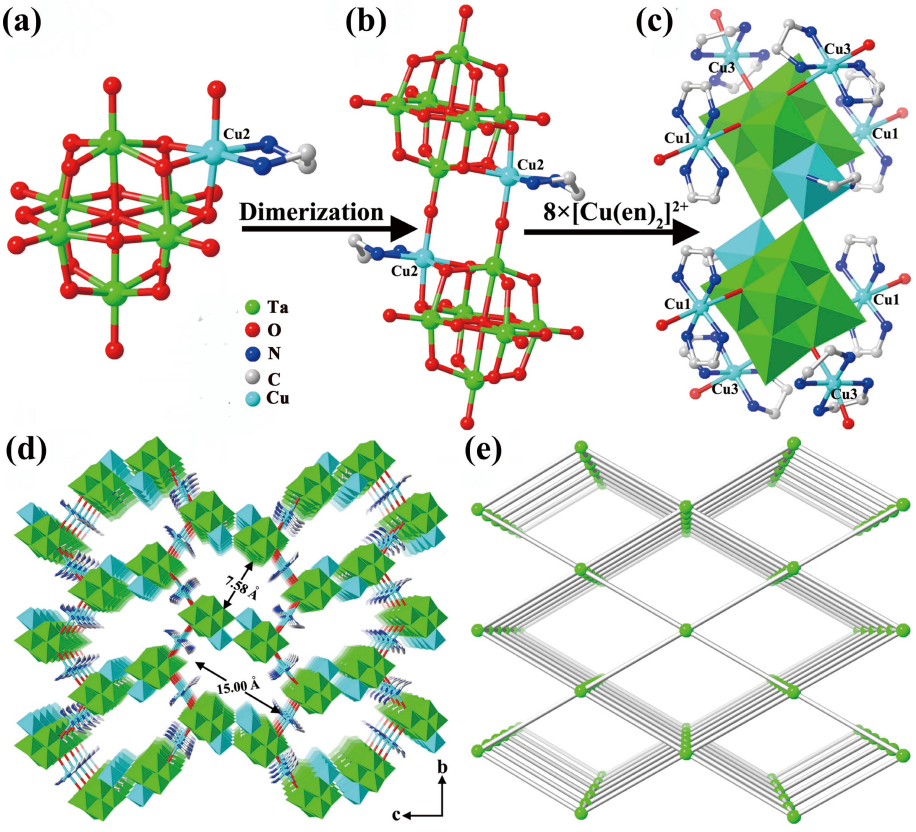

Figure 8 (a) $[Cu(en)(Ta_6O_{19})]^{6-}$ cluster; (b) structure of the $\{CuTa_6\}_2$ SBU; (c) coordination environment of the $\{CuTa_6\}_2$ SBU; (d) view of the 3D framework structure in $H_2[Cu(en)_2(H_2O)_2]\{[Cu(en)_2]_4[Cu(en)(Ta_6O_{19})]_2\}\cdot 14H_2O$; (e) 3D topology of $H_2[Cu(en)_2(H_2O)_2]\{[Cu(en)_2]_4[Cu(en)(Ta_6O_{19})]_2\}\cdot 14H_2O$. Polyhedral codes: TaO_6, green; CuO_2N_4/CuO_4N_2, cyan. Reproducted with permission from Ref. [48], © The Royal Society of Chemistry 2019.

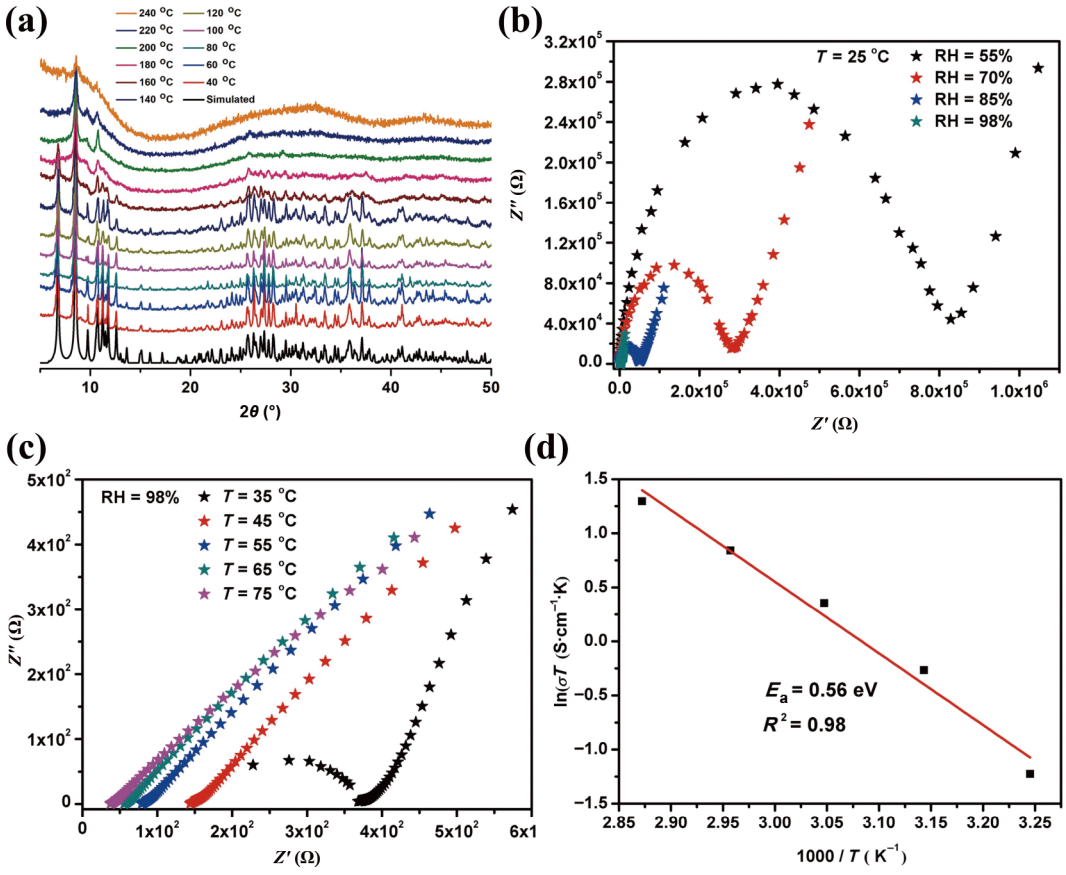

Figure 9 (a) Variable-temperature powder X-ray diffraction patterns of $H_2[Cu(en)_2(H_2O)_2]\{[Cu(en)_2]_4[Cu(en)(Ta_6O_{19})]_2\}\cdot 14H_2O$; (b) Nyquist plots of $H_2[Cu(en)_2(H_2O)_2]\{[Cu(en)_2]_4[Cu(en)(Ta_6O_{19})]_2\}\cdot 14H_2O$ under different relative humidity (RH) conditions at 25 °C; (c) Nyquist plots of $H_2[Cu(en)_2(H_2O)_2]\{[Cu(en)_2]_4[Cu(en)(Ta_6O_{19})]_2\}\cdot 14H_2O$ under different temperature conditions at 98% RH; (d) Arrhenius plots and linear fitting of temperature-dependence proton conduction at 98% RH. Reproducted with permission from Ref. [48], © The Royal Society of Chemistry 2019.

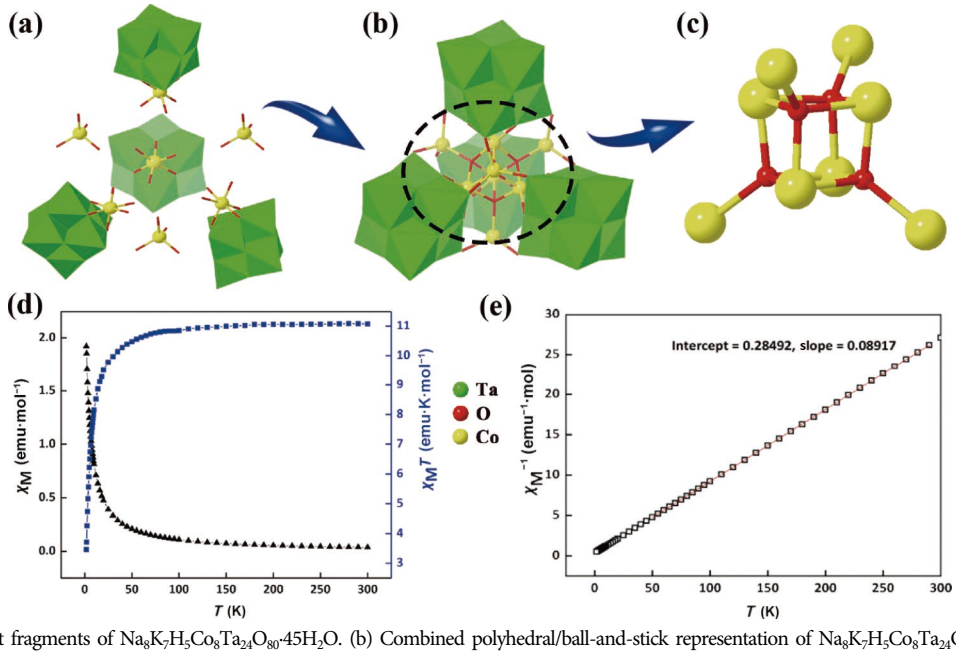

Figure 10 (a) Different fragments of $Na_8K_7H_5Co_8Ta_{24}O_{80}\cdot 45H_2O$. (b) Combined polyhedral/ball-and-stick representation of $Na_8K_7H_5Co_8Ta_{24}O_{80}\cdot 45H_2O$. (c) Ball-and-stick representation of $\{Co_8\}$. (d) Temperature-dependence of the molar magnetic susceptibility χ_M and the product $\chi_M T$ for $Na_8K_7H_5Co_8Ta_{24}O_{80}\cdot 45H_2O$. (e) Plot of χ_M^{-1} versus temperature between 300 and 50 K of $Na_8K_7H_5Co_8Ta_{24}O_{80}\cdot 45H_2O$. Polyhedral codes: TaO_6, green. Reproducted with permission from Ref. [51], © American Chemical Society 2018.

noted that the oxidation state of the four-coordinated Co ions is +2, whereas that of the six-coordinated Co ions in the cubane $\{Co_4O_4\}$ is +3. $[H_5Co_8Ta_{24}O_{80}]^{15-}$ is the largest high-nuclearity Co-containing POTa obtained thus far [51]. The compound was synthesized using a water-bath in combination with diffusion, further proving that diffusion plays an important role in the formation of POTas. At the same time, the synthesis of this compound also demonstrated that the O_b atoms and O_t atoms of POTas have similar structures and coordination capabilities to those of PONbs. The magnetic susceptibilities of $Na_8K_7H_5Co_8Ta_{24}O_{80}{\cdot}45H_2O$ follow the Curie–Weiss law with antiferromagnetic properties.

Other example of a derivative of **Ta_6** is a POTa in which the **Ta_6** conformation is broken. In 2013, Yagasaki et al. demonstrated that the TBA salt of $[H_2Ta_6O_{19}]^{6-}$ yields decatantalate $[Ta_{10}O_{28}]^{6-}$ (**Ta_{10}**) when heated in toluene [38]. The **Ta_{10}** anion can be regarded as two classical **Ta_6** polyoxoanion building blocks losing a $\{TaO_6\}$ octahedron octahedral and then bridging together (Fig. 11(a)). The **Ta_{10}** anion is isostructural with $[V_{10}O_{28}]^{6-}$ and $[Nb_{10}O_{28}]^{6-}$, which exhibit an *mmm* (D_{2h}) symmetry. In addition, the **Ta_{10}** and $[Nb_{10}O_{28}]^{6-}$ anions are identical, with only slight differences in their M–O bond lengths. Both **Ta_{10}** and $[Nb_{10}O_{28}]^{6-}$ are much larger than $[V_{10}O_{28}]^{6-}$. This fascinating discovery indicates that these compounds having completely different structures need the same amount of acid or protons. The average charge per Ta atom of **Ta_{10}** (−0.60) is very similar to that of $[H_{18}(Ta_6O_{19})_4]^{14-}$ (−0.58). **Ta_{10}** was formed after prolonged heating of the solution, whereas in the formation of $[H_{18}(Ta_6O_{19})_4]^{14-}$, the reaction solution was only heated for one night. More importantly, kinetic control seemed to contribute to the formation of different POTas. To sum up, the synthesis of **Ta_{10}** has provided a clear clue for inorganic chemists to obtain other novel structures in the near future, allowing a series of exploratory studies on POTas in nonaqueous media.

In 2016, Casey and his coworkers reported two Ti-substituted POTa, i.e., $[Ti_2Ta_8O_{28}]^{8-}$ and $[Ti_{12}Ta_6O_{44}]^{10-}$ [49], which broadened the pH range of tantalates in aqueous solution. These Ti-substituted POTa clusters share similarities with previously reported niobates but are slightly larger and more stable in solution. In light of the synthetic success of Ti-substituted polyoxoniobates, these authors expected that a similar strategy could be adopted to prepare Ti-substituted POTas. As a result, they obtained the first soluble Ti^{IV}-disubstituted decatantalate–oxo clusters, namely, $TMA_8Ti_2Ta_8O_{28}{\cdot}21H_2O$ (**Ti_2Ta_8**) and the super-octahedral cluster of $TMA_{10}Ti_{12}Ta_6O_{44}{\cdot}39H_2O$ (**$Ti_{12}Ta_6$**). It is worth noting that hydrous tantalum oxide is used in the synthesis process instead of the Ta_6O_{19} precursor. This work paved the way for the use of hydrous tantalum oxide to synthesize novel POTas. It was intriguing to find that **$Ti_{12}Ta_6$** could be isolated from **Ti_2Ta_8** on account of its slightly lower solubility, but the amount of **$Ti_{12}Ta_6$** in the product was much smaller than that of **Ti_2Ta_8**. At the same time, Ti_2Ta_8 was found to transform into **$Ti_{12}Ta_6$** under hydrothermal conditions when an excess of Ti^{IV} source was added to the solution. In addition, the **$Ti_{12}Ta_6$** cluster could also be converted to **Ti_2Ta_8** by controlling the pH with TMAOH under hydrothermal treatment.

The structure of **$Ti_{12}Ta_6$** can be described as a $[Ti_{12}O_{38}]^{28-}$ core capped with six Ta=O groups, and the six oxo groups in the cluster are bonded to six Ta^V sites at the corners of the super-octahedral **$Ti_{12}Ta_6$** structure. This structure shows that six capping tantanyl groups can stabilize the otherwise hydrolytically unstable $[Ti_{12}O_{38}]^{28-}$ cluster. The **$Ti_{12}Ta_6$** cluster has a vacancy in the center surrounded by six oxygen ligands. Moreover, the Ti_2Ta_8 polyoxoanion also has two Ti sites occupying the center position (Figs. 12(b)–12(f)).

In 2017, Niu et al. reported two 6-peroxotantalo-4-phosphates: $Cs_3[H_9P_4Ta_6(O_2)_6O_{25}]{\cdot}9H_2O$ (***cis*-P_4Ta_6**) and $(CN_3H_6)_6[H_4P_4Ta_6(O_2)_6O_{24}]{\cdot}4H_2O$ (***trans*-P_4Ta_6**) [50]. Using a combination of synthetic strategies, the author skillfully used the peroxo group to protect the Ta-O framework to avoid the hydrolysis of POTas. More importantly, the pH value and the nature of the cations (Ce and guanidinium ion) were found to play vital roles in the formation of these compounds, with different pH conditions resulting in different P_4Ta_6 configurations. Both molecular structures consist of two identical P_2Ta_3, which can be regarded as a peroxohexatantalate fragment with a contiguous longitudinal strip of three $Ta(O_2)$ groups replaced with two PO_4 groups. **$P_4Ta_6O_{25}$** consists of two identical P_2Ta_3 subunits connected through three μ_2-O bridging ligands to form a basket-shaped architecture with an idealized C_{2v} symmetry. **$P_4Ta_6O_{24}$** can be viewed as two P_2Ta_3 units fused by two Ta–μ_2-O–Ta and two P–μ_2-O–Ta bridges. In 2019, Niu followed a one-pot synthetic assembly approach to isolate a series of eight isostructural compounds of formula $Cs_3[Ln(H_2O)_6\{H_4(TaO_2)_6As_4O_{24}\}]{\cdot}7H_2O$ (Ln = Sm, Eu, Tb, Dy, Er, Tm, Yb, Lu) (**As_4Ta_6-Ln**) [52]. These compounds represent the first class of "pure" POTa-based lanthanide derivatives. In 2021, $KNa_2[HSe_2(TaO_2)_6(OH)_4(H_2O)_2O_{13}]{\cdot}15H_2O$ (**Se_2Ta_6**) and $Cs_2K_{1.5}Na_{1.5}[Se_4(TaO_2)_6(OH)_3O_{18}]{\cdot}17H_2O$ (**Se_4Ta_6**) were successfully prepared by Du. The structure of **Se_4Ta_6** is very similar to that of **P_4Ta_6** and constitutes the first example of the introduction of Se into a POTa (Fig. 12). Shortly after that, Du successfully prepared $CsK[Ln(H_2O)_6Se_4(TaO_2)_6(OH)_3O_{18}]{\cdot}nH_2O$ (**Se_4Ta_6-Ln**), which shares structural similarities with **P_4Ta_6** but with slight differences: i) the two equatorial Se atoms are in the same direction instead of the opposite direction in **P_4Ta_6**; ii) Se is tricoordinated, whereas P is tetracoordinated [55]. Moreover, $Cs_3H_3[Ni_2(H_2O)_4\{P_4Ta_6(O_2)_6O_{24}\}]{\cdot}7H_2O$, $Cs_3NaH_4[Zn(H_2O)_4\{P_4Ta_6(O_2)_6O_{24}\}]{\cdot}13H_2O$, and $Cs_3NaH_4[Cd(H_2O)_4\{P_4Ta_6(O_2)_6O_{24}\}]{\cdot}8H_2O$, which derive from the structure of **P_4Ta_6**, were successfully prepared in 2022. These three compounds were obtained when Cs^+ countercations were used, thus demonstrating that the nature of the countercation has a strong influence on the crystallization of POTas [54]. It is noteworthy that some tantalum-oxo cluster incorporated POTs have also been reported in recent years. The mixed-addenda Ta/W POMs have also enriched the limited tantalum chemistry. For example, in 2012, Liu's group first reported four mixed-addenda Ta/W POTs, namely, $K_5Na_4[P_2W_{15}O_{59}(TaO_2)_3]{\cdot}17H_2O$, $K_8Na_8H_4[P_8W_{60}Ta_{12}(H_2O)_4(OH)_8O_{236}]{\cdot}42H_2O$, $Cs_3K_{3.5}H_{0.5}[SiW_9(TaO_2)_3O_{37}]{\cdot}9H_2O$, and $Cs_{10.5}K_4H_{5.5}[Ta_4O_6(SiW_9Ta_3O_{40})_4]{\cdot}30H_2O$ [62]. Later, Su's group reported other two mixed-addenda Ta/W POMs, i.e., $Cs_5K_4\{Cr_3[Ta_3P_2W_{15}O_{62}]_2(H_2O)_{12}\}{\cdot}15H_2O$ and $Cs_{8.5}K_8Na_2H_{5.5}\{Cr_4[Ta_3P_2W_{15}O_{62}]_4(H_2O)_{12}\}{\cdot}53H_2O$ [63]. In 2018, a family of rare earth-containing mixed-addenda Ta/W POMs exhibiting remarkable heterogeneous catalytic activity for cyanosilylation, that is, $[RE(H_2O)_7]_3{-}P_2W_{15}Ta_3O_{62}{\cdot}nH_2O$ (RE = Y, Eu, Gd, Tb, Dy, Ho, Er, Tm, Yb, and Lu), was created by Chen and coworkers [64] More recently, the same group reported $(NH_4)_{41}H_7[K_3(H_2O)_3(P_2W_{15}Ta_3O_{62})_6(Mo_2O_4CH_3CO_2)_3(MoO_3)_2]{\cdot}85H_2O$ as the first Mo/Ta/W ternary mixed-addenda POM, which was proved to be an efficient photocatalyst under simulated sunlight [65].

4 Summary

In this review, recent advances of POTas are presented. The known

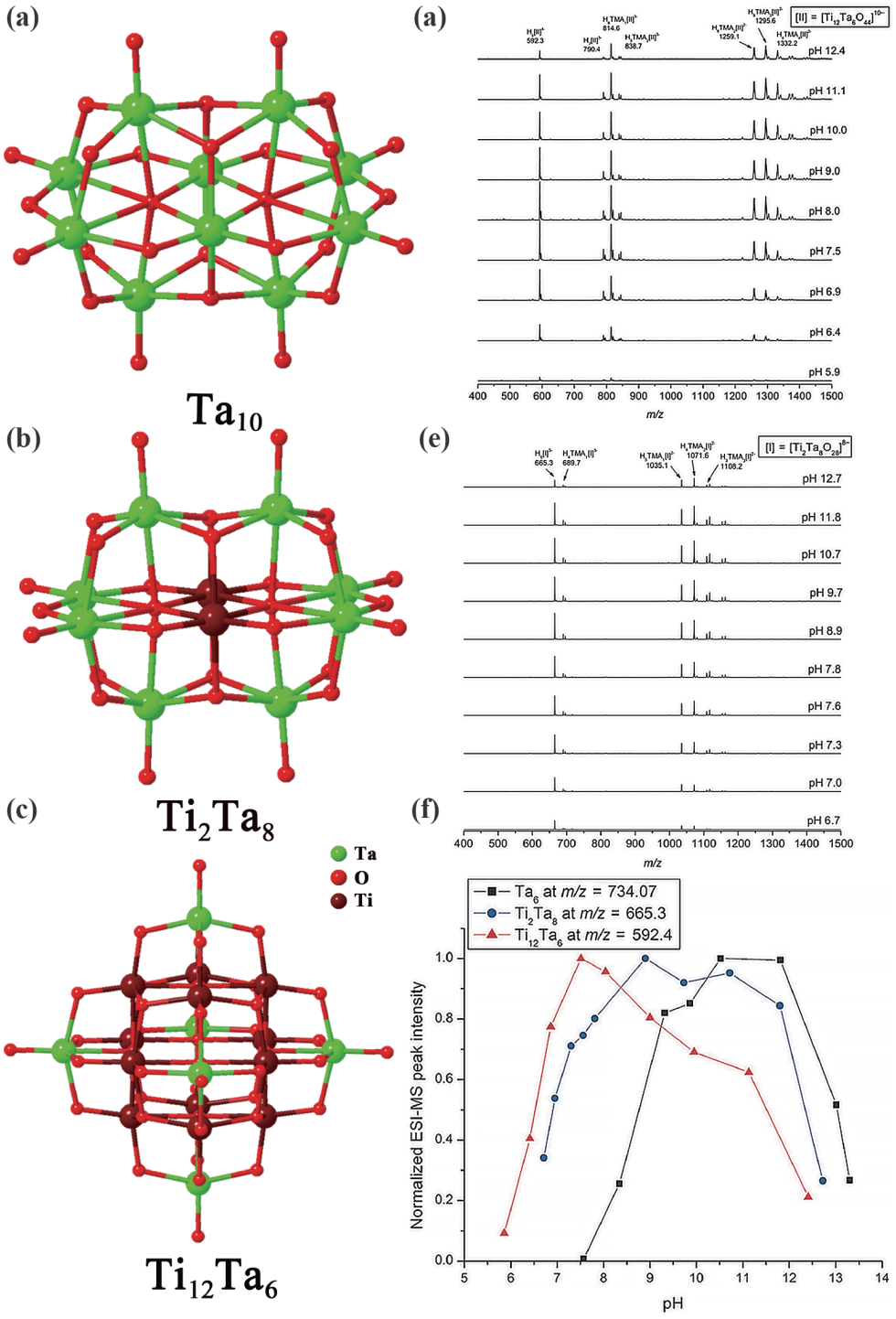

Figure 11 (a) Ball-and-stick representation of the Ta_{10} cluster polyanion. (b) Ball-and-stick representation of the $Ti_{12}Ta_6$ cluster polyanion. (c) Ball-and-stick representation of the Ti_2Ta_8 cluster polyanion. (d) ESI-MS spectra of $Ti_{12}Ta_6$ solutions as a function of pH. (e) ESI-MS spectra of Ti_2Ta_8 solutions as a function of pH. (f) pH-dependent stabilities of Ta_6, Ti_2Ta_8, and $Ti_{12}Ta_6$ determined by ESI-MS. Reproducted with permission from Ref. [49], © WILEY-VCH Verlag GmbH & Co. KGaA, Weinheim 2016.

POTas have been classified into four categories according to the types of counterions and configurations of the cluster skeleton. Besides, the synthetic strategies for POTas are discussed. Notably, despite the recent progress, POTas are still in their infancy, and further development requires considering some issues. For example, 1) the structural diversity of POTas remains quite limited compared with that of POTs, POMos, POVs, and PONbs; 2) the metal nuclearity of POTas is still much smaller than that of other POM members; 3) the overwhelming majority of POTas were prepared in aqueous environment; 4) the properties and applications of POTas have not been extensively studied. These limitations can be attributed to synthetic difficulties, the limited stability of most POTas in acidic/neutral environments, and the scarce reactivity of the Ta atoms in POTas with a constant

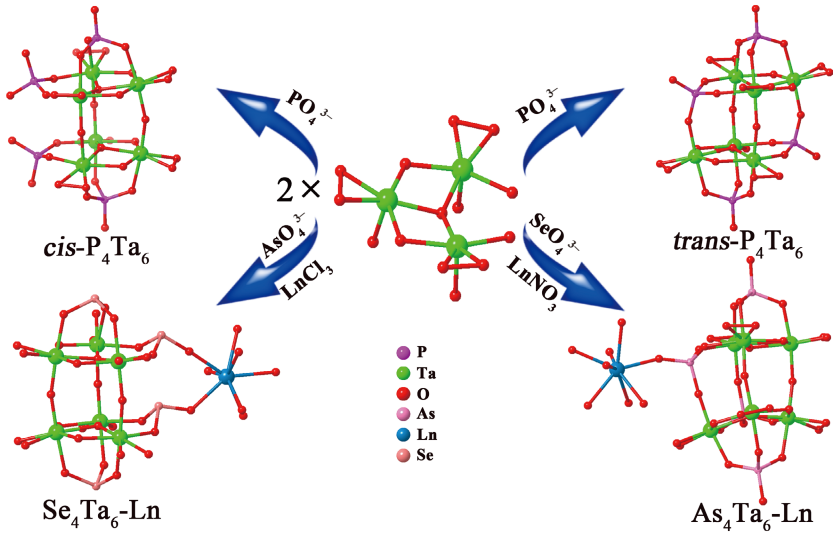

Figure 12 Ball-and-stick representations of As_4Ta_6-Ln, *cis*-P_4Ta_6, *trans*-P_4Ta_6, and Se_4Ta_6-Ln.

oxidation state of +5. Therefore, future studies should involve the following aspects: 1) introducing more transition metals into POTas to enrich their structural diversity; 2) using diverse organic ligands to assembly POTa clusters into extended materials; 3) exploring other synthetic strategies in organic media; 4) combining POTas with other materials to realize a wide range of properties and applications. This review could offer some useful references, experience, and practical guidance for further development of POTas.

Acknowledgment

This work was supported by the National Natural Science Foundation of China (Nos. 22171045, 92161108 and 21971039), the Natural Science Fund of Fujian Province (No. 2020J01438) and the Key Program of Natural Science Foundation of Fujian Province (No. 2021J02007).

Declaration of competing interest

The authors have no competing interests to declare that are relevant to the content of this article.

Author contribution statement

The manuscript was written through contributions of all authors.

References

[1] Zhang, D. D.; Li, H.; Li, C.; Wang, Z. H.; Li, T.; Li, N.; Cheng, M. Y.; Wang, J. P.; Niu, J. Y.; Liu, T. B. A large molecular cluster with high proton release capacity. *Chem. Commun.* **2020**, *56*, 12849–12852.

[2] Yang, G. P.; Zhang, X. L.; Liu, Y. F.; Zhang, D. D.; Li, K.; Hu, C. W. Self-assembly of Keggin-type U(VI)-containing tungstophosphates with a sandwich structure: An efficient catalyst for the synthesis of sulfonyl pyrazoles. *Inorg. Chem. Front.* **2021**, *8*, 4650–4656.

[3] Cheng, M. Y.; Liu, Y. F.; Du, W. X.; Shi, J. W.; Li, J. H.; Wang, H. Y.; Li, K.; Yang, G. P.; Zhang, D. D. Two Dawson-type U(VI)-containing selenotungstates with sandwich structure and its high-efficiency catalysis for pyrazoles. *Chin. Chem. Lett.* **2022**, *33*, 3899–3902.

[4] Cheng, M. Y.; Liu, Y. F.; Li, N.; Shi, J. W.; Du, W. X.; Zhang, D. D.; Yang, G. P.; Wang, G.; Niu, J. Y. Two novel telluroniobates with efficient catalytic activity for the imidation/amidation reaction. *Chem. Commun.* **2022**, *58*, 1167–1170.

[5] Shimoyama, Y.; Ogiwara, N.; Weng, Z. W.; Uchida, S. Oxygen evolution reaction driven by charge transfer from a Cr complex to co-containing polyoxometalate in a porous ionic crystal. *J. Am. Chem. Soc.* **2022**, *144*, 2980–2986.

[6] Xiao, H. P.; Hao, Y. S.; Li, X. X.; Xu, P.; Huang, M. D.; Zheng, S. T. A water-soluble antimony-rich polyoxometalate with broad-spectrum antitumor activities. *Angew. Chem., Int. Ed.* **2022**, *61*, e202210019.

[7] Bontchev, R. P., Venturini, E. L., Nyman, M. Copper-linked hexaniobate lindqvist clusters-variations on a theme. *Inorg. Chem.* **2007**, *46*, 4483–4491.

[8] Khan, M. I. Novel extended solids composed of transition metal oxide clusters. *J. Solid State Chem.* **2000**, *152*, 105–112.

[9] Pope, M. T.; Müller, A. Polyoxometalate chemistry: An old field with new dimensions in several disciplines. *Angew. Chem., Int. Ed.* **1991**, *30*, 34–48.

[10] Bi, L. H.; Reicke, M.; Kortz, U.; Keita, B.; Nadjo, L.; Clark, R. J. First structurally characterized palladium(II)-substituted polyoxoanion: $[Cs_2Na(H_2O)_{10}Pd_3(\alpha\text{-}Sb^{III}W_9O_{33})_2]^{9-}$. *Inorg. Chem.* **2004**, *43*, 3915–3920.

[11] Kortz, U.; Savelieff, M. G.; Bassil, B. S.; Keita, B.; Nadjo, L. Synthesis and characterization of iron(III)-substituted, dimeric polyoxotungstates, $[Fe_4(H_2O)_{10}(\beta\text{-}XW_9O_{33})_2]^{n-}$ (n = 6, X = As^{III}, Sb^{III}; n = 4, X = Se^{IV}, Te^{IV}). *Inorg. Chem.* **2002**, *41*, 783–789.

[12] Laronze, N. ; Marrot, J. ; Hervé, G. Cation-directed synthesis of tungstosilicates. 1. Syntheses and structures of $K_{10}A\text{-}\alpha\text{-}[SiW_9O_{34}]\cdot 24H_2O$, of the sandwich-type complex $K_{10.75}[Co(H_2O)_6]_{0.5}[Co(H_2O)_4Cl]_{0.25}A\text{-}\alpha\text{-}[K_2\{Co(H_2O)_2\}_3(SiW_9O_{34})_2]\cdot 32H_2O$ and of $Cs_{15}[K(SiW_{11}O_{39})_2]\cdot 39H_2O$. *Inorg. Chem.* **2003**, *42*, 5857–5862.

[13] Zhu, Z. K.; Zhang, J.; Cong, Y. C.; Ge, R.; Li, Z.; Li, X. X.; Zheng, S. T. Two giant calixarene-like polyoxoniobate nanocups $\{Cu_{12}Nb_{120}\}$ and $\{Cd_{16}Nb_{128}\}$ built from mixed macrocyclic cluster motifs. *Angew. Chem., Int. Ed.* **2022**, *61*, e202113381.

[14] Wu, Y. L.; Li, X. X.; Qi, Y. J.; Yu, H.; Jin, L.; Zheng, S. T. $\{Nb_{288}O_{768}(OH)_{48}(CO_3)_{12}\}$:A macromolecular polyoxometalate with close to 300 niobium atoms. *Angew Chem., Int. Ed.* **2018**, *57*, 8572–8576.

[15] Fang, X. K.; Kögerler, P.; Furukawa, Y.; Speldrich, M.; Luban, M. Molecular growth of a core-shell polyoxometalate. *Angew. Chem., Int. Ed.* **2011**, *50*, 5212–5216.

[16] Gupta, S. K.; Gupta, A. K.; Yadav, R. K.; Singh, A.; Yadav, B. C. Highly efficient S-g-CN/Mo-368 catalyst for synergistically NADH regeneration under solar light. *Photochem. Photobiol.* **2022**, *98*, 160–168.

[17] Pickhard, F.; Hart, H. Die kristallstrukturen von $K_8Ta_6O_{19}\cdot 16H_2O$ und $K_7NaTa_6O_{19}\cdot 14H_2O$. *Z. Anorg. Allg. Chem.* **1997**, *623*, 1311–1316.

[18] Nelson, W. H.; Tobias, R. S. Structure of the polyanions of the transition metals in aqueous solution: The hexatantalate. *Inorg. Chem.* **1963**, *2*, 985–992.

[19] Anderson, T. M.; Rodriguez, M. A.; Bonhomme, F.; Bixler, J. N.; Alam, T. M.; Nyman, M. An aqueous route to $[Ta_6O_{19}]^{8-}$ and solid-state studies of isostructural niobium and tantalum oxide complexes. *Dalton Trans* **2007**, 4517–4522

[20] Abramov, P. A.; Abramova, A. M.; Peresypkina, E. V.; Gushchin, A. L.; Adonin, S. A.; Sokolov, M. N. New polyoxotantalate salt $Na_8[Ta_6O_{19}]\cdot 245H_2O$ and its properties. *J. Struct. Chem* **2011**, *52*, 1012–1017.

[21] Lindqvist, I.; Aronsson, B. The structure of the hexatantalate ion in $4K_2O\cdot 3Ta_2O_5\cdot 16H_2O$. *Ark. For Kemi* **1953**, *7*, 49–52.

[22] Nyman, M.; Anderson, T. M.; Provencio, P. P. Comparison of aqueous and non-aqueous soft-chemical syntheses of lithium niobate and lithium tantalate powders. *Cryst. Growth Des.* **2009**, *9*, 1036–1040.

[23] Huang, P.; Qin, C.; Zhou, Y.; Hong, Y. M.; Wang, X. L.; Su, Z. M. Self-assembly and photocatalytic H_2 evolution activity of two unprecedented polytantalotungstates based on the largest $\{Ta_{18}\}$ and $\{Ta_{18}Yb_2\}$ clusters. *Chem. Commun.* **2016**, *52*, 13787–13790.

[24] Nyman, M. Polyoxoniobate chemistry in the 21st century. *Dalton Trans.* **2011**, *40*, 8049–8058.

[25] Fullmer, L. B.; Malmberg, C. E.; Fast, D. B.; Wills, L. A.; Cheong, P. H. Y.; Dolgos, M. R.; Nyman, M. Aqueous tantalum polyoxometalate reactivity with peroxide. *Dalton Trans.* **2017**, *46*, 8486–8493.

[26] Monakhov, K. Y.; Bensch, W.; Kögerler, P. Semimetal-functionalised polyoxovanadates. *Chem. Soc. Rev.* **2015**, *44*, 8443–8483.

[27] Zhao, H. Y.; Li, Y. Z.; Zhao, J. W.; Wang, L.; Yang, G. Y. State-of-the-art advances in the structural diversities and catalytic applications of polyoxoniobate-based materials. *Coord. Chem. Rev.* **2021**, *443*, 213966.

[28] Liu, J. C.; Zhao, J. W.; Streb, C.; Song, Y. F. Recent advances on high-nuclear polyoxometalate clusters. *Coord. Chem. Rev.* **2022**, *471*, 214734.

[29] Yu, H.; Zheng, S. T. Research advances of polyoxotantalates. *Chin. Sci. Bull.* **2018**, *63*, 3277–3285.

[30] Liu, R. L.; Yu, Y. H.; Wang, H. W.; Liu, Y. Y.; Li, G. High and tunable proton conduction in six 3D-substituted imidazole dicarboxylate-based lanthanide-organic frameworks. *Inorg. Chem.* **2021**, *60*, 10808–10818.

[31] Hegetschweiler, K.; Raber, T.; Reiss, G. J.; Frank, W.; Wörle, M.; Currao, A.; Nesper, R.; Kradolfer, T. A polyoxo-polyolato complex of tantalum (V) with a double adamantane-like $[Ta_7O_{12}]^{11+}$ core. *Angew. Chem., Int. Ed.* **1997**, *36*, 1964–1966.

[32] Hartl, H.; Pickhard, F.; Emmerling, F.; Röhr, C. Rubidium- und caesium-verbindungen mit dem isopolyanion $[Ta_6O_{19}]^{8-}$—Synthesen, kristallstrukturen, thermische und schwingungsspektroskopische untersuchungen der oxotantalate $A_8[Ta_6O_{19}]\cdot n\ H_2O$ (A = Rb, Cs; n = 0, 4, 14). *Z. Anorg. Allg. Chem.* **2001**, *627*, 2630–2638.

[33] Shen, L.; Xu, Y. Q.; Gao, Y. Z.; Cui, F. Y.; Hu, C. W. 3D extended polyoxoniobates/tantalates solid structure: Preparation, characterization and photocatalytic properties. *J. Mol. Struct.* **2009**, *934*, 37–43.

[34] Britvin, S. N.; Siidra, O. I.; Lotnyk, A.; Kienle, L.; Krivovichev, S. V.; Depmeier, W. The fluoride route to Lindqvist clusters: Synthesis and crystal structure of layered hexatantalate $Na_8Ta_6O_{19}\cdot 26H_2O$. *Inorg. Chem. Commun.* **2012**, *25*, 18–20.

[35] Matsumoto, M.; Ozawa, Y.; Yagasaki, A. Which is the most basic oxygen in $[Ta_6O_{19}]^{8-}$?—Synthesis and structural characterization of $[H_2Ta_6O_{19}]^{6-}$. *Inorg. Chem. Commun.* **2011**, *14*, 115–117.

[36] Ban, T.; Yoshikawa, S.; Ohya, Y. Synthesis of layered tantalate nanocrystals by aqueous process at room temperature. *CrystEngComm.* **2012**, *14*, 7709–7714.

[37] Matsumoto, M.; Ozawa, Y.; Yagasaki, A. Long hydrogen-bonded rod of molecular oxide: A hexatantalate tetramer. *Inorg. Chem.* **2012**, *51*, 5991–5993.

[38] Matsumoto, M.; Ozawa, Y.; Yagasaki, A.; Zhe, Y. Decatantalate-the last member of the group 5 decametalate family. *Inorg. Chem.* **2013**, *52*, 7825–7827.

[39] Besserguenev, A. V.; Dickman, M. H.; Pope, M. T. Robust, alkali-stable, triscarbonyl metal derivatives of hexametalate anions, $[M_6O_{19}\{M'(CO)_3\}_n]^{(8-n)-}$ (M = Nb, Ta; M' = Mn, Re; n = 1, 2). *Inorg. Chem.* **2001**, *40*, 2582–2586.

[40] Guo, G. L.; Xu, Y. Q.; Chen, B. K.; Lin, Z. G.; Hu, C. W. Two novel polyoxotantalates formed by Lindqvist-type hexatantalate and Copper-amine complexes. *Inorg. Chem. Commun.* **2011**, *14*, 1448–1451.

[41] Abramov, P. A.; Sokolov, M. N.; Floquet, S.; Haouas, M.; Taulelle, F.; Cadot, E.; Peresypkina, E. V.; Virovets, A. V.; Vicent, C.; Kompankov, N. B. et al. Coordination-induced condensation of $[Ta_6O_{19}]^{8-}$: Synthesis and structure of $[\{(C_6H_6)Ru\}_2Ta_6O_{19}]^{4-}$ and $[\{(C_6H_6)RuTa_6O_{18}\}_2(\mu\text{-}O)]^{10-}$. *Inorg. Chem.* **2014**, *53*, 12791–12798.

[42] Hu, P.; Wang, X. F.; Ma, Y.; Wang, Q. L.; Li, L. C.; Liao, D. Z. A new family of Ln-radical chains (Ln = Nd, Sm, Gd, Tb and Dy): Synthesis, structure, and magnetic properties. *Dalton Trans.* **2014**, *43*, 2234–2243.

[43] Abramov, P. A.; Vicent, C.; Kompankov, N. B.; Gushchin, A. L.; Sokolov, M. N. Coordination of $\{C_5Me_5Ir\}^{2+}$ to $[M_6O_{19}]^{8-}$ (M = Nb, Ta)—Analogies and differences between Rh and Ir, Nb and Ta. *Eur. J. Inorg. Chem.* **2016**, *2016*, 154–160.

[44] Li, S. Z.; Chen, S. M.; Zhang, F. L.; Li, Z. Y.; Zhang, C.; Cao, G. X.; Zhai, B. Synthesis and characterization of two polyoxotantalates: A building block and its dimeric. *Inorg. Chem. Commun.* **2019**, *106*, 228–232.

[45] Ma, Y. C.; Sun, J. J.; Li, C.; Li, N.; Ma, P. T.; Zhang, D. D.; Wang, G.; Niu, J. Y. Assembly of two hybrid organic-inorganic hexatantalate. *Inorg. Chem. Commun.* **2019**, *101*, 6–10.

[46] Krause, D. C.; Mangelsen, S.; Näther, C.; Bensch, W. Synthesis, crystal structure and selected properties of $K_2[Ni(dien)_2]\{[Ni(dien)]_2Ta_6O_{19}\}\cdot 11H_2O$. *Z. Naturforschm. B* **2021**, *76*, 775–782.

[47] Krause, D. C.; Mangelsen, S.; Näther, C.; Bensch, W. Synthesis and selected properties of new complex cation decorated polyoxotantalates. *Cryst. Growth Des.* **2021**, *21*, 7128–7138.

[48] Li, Z.; Zhang, J.; Lin, L. D.; Liu, J. H.; Li, X. X.; Zheng, S. T. Inorganic-organic hybrid high-dimensional polyoxotantalates and their structural transformations triggered by water. *Chem. Commun.* **2019**, *55*, 11735–11738.

[49] Son, J. H.; Casey, W. H. Titanium-substituted polyoxotantalate clusters exhibiting wide pH stabilities: $[Ti_2Ta_8O_{28}]^{8-}$ and $[Ti_{12}Ta_6O_{44}]^{10-}$. *Chem.—Eur. J.* **2016**, *22*, 14155–14157.

[50] Zhang, D. D.; Liang, Z. J.; Liu, S. Y.; Li, L. S.; Ma, P. T.; Zhao, S. F.; Wang, H. Y.; Wang, J. P.; Niu, J. Y. Discovery of heteropolytantalate: Synthesis and structure of two 6-peroxotantalo-4-phosphate clusters. *Inorg. Chem.* **2017**, *56*, 5537–5543.

[51] Liang, Z. J.; Zhao, S. F.; Ma, P. T.; Zhang, C.; Sun, J. J.; Song, T. T.; Niu, J. Y.; Wang, J. P. A novel tetrameric polyoxotantalate aggregate: $\{Co_8Ta_{24}\}$ featuring a high-nuclearity Co_8 cluster. *Inorg. Chem.* **2018**, *57*, 12471–12474.

[52] Liang, Z. J.; Wu, H. C.; Singh, V.; Qiao, Y. Y.; Li, M. M.; Ma, P. T.; Niu, J. Y.; Wang, J. P. Assembly of lanthanide-containing polyoxotantalate clusters with efficient photoluminescence properties. *Inorg. Chem.* **2019**, *58*, 13030–13036.

[53] Du, W. X.; Cheng, M. Y.; Li, K.; Ma, Y. C.; Shi, J. W.; Zhang, D. D. Insight into hexanuclear peroxotantalum complexes: Synthesis,

characterization, and efficient catalyst for amidation reaction. *Tungsten* **2022**, *4*, 158–167.
[54] Li, X.; Zhao, H.; Li, Y. Y.; Yang, Y. Y.; Zhang, M. Y.; Liu, S. Y.; Ma, P. T.; Wang, J. P.; Niu, J. Y. Synthesis, structure and properties of three novel transition-metal-containing tantalum-phosphate clusters. *Chin. Chem. Lett.* **2022**, *33*, 4675–4678.
[55] Du, W. X.; Liu, Y. F.; Sun, J. J.; Wang, H. Y.; Yang, G. P.; Zhang, D. D. Three rare-earth incorporating 6-peroxotantalo-4-selenates and catalytic activities for imidation reaction. *Dalton Trans.* **2022**, *51*, 9988–9993.
[56] Filowitz, M.; Ho, R. K. C.; Klemperer, W. G.; Shum, W. Oxygen-17 nuclear magnetic resonance spectroscopy of polyoxometalates 1. Sensitivity and resolution. *Inorg. Chem.* **1979**, *18*, 93–103.
[57] Putaj, P.; Lefebvre, F. Polyoxometalates containing late transition and noble metal atoms. *Coord. Chem. Rev.* **2011**, *255*, 1642–1685.
[58] Izarova, N. V.; Pope, M. T.; Kortz, U. Noble metals in polyoxometalates. *Angew. Chem., Int. Ed.* **2012**, *51*, 9492–9510.
[59] Sartorel, A.; Carraro, M.; Scorrano, G.; Zorzi, R. D.; Geremia, S.; McDaniel, N. D.; Bernhard, S.; Bonchio, M. Polyoxometalate embedding of a tetraruthenium(IV)-oxo-core by template-directed metalation of $[\gamma\text{-}SiW_{10}O_{36}]^{8-}$: A totally inorganic oxygen-evolving catalyst. *J. Am. Chem. Soc.* **2008**, *130*, 5006–5007.
[60] Walter, M. G.; Warren, E. L.; McKone, J. R.; Boettcher, S. W.; Mi, Q. X.; Santori, E. A.; Lewis, N. S. Solar water splitting cells. *Chem. Rev.* **2010**, *110*, 6446–6473.
[61] Youngblood, W. J.; Lee, S. H. A.; Kobayashi, Y.; Hernandez-Pagan, E. A.; Hoertz, P. G.; Moore, T. A.; Moore, A. L.; Gust, D.; Mallouk, T. E. Photoassisted overall water splitting in a visible light-absorbing dye-sensitized photoelectrochemical cell. *J. Am. Chem. Soc.* **2009**, *131*, 926–927.
[62] Li, S. J.; Liu, S. M.; Liu, S. X.; Liu, Y. W.; Tang, Q.; Shi, Z.; Ouyang, S. X.; Ye, J. H. $\{Ta_{12}\}/\{Ta_{16}\}$ cluster-containing polytantalotungstates with remarkable photocatalytic H_2 evolution activity. J Am. *Chem. Soc.* **2012**, *134*, 19716–19721.
[63] Huang, P.; Wang, X. J.; Qi, J. J.; Wang, X. L.; Huang, M.; Wu, H. Y.; Qin, C.; Su, Z. M. Self-assembly and photocatalytic H_2 evolution activity of two nanoscale polytantalotungstates based on unprecedented $\{Cr_3Ta_6\}$ and $\{Cr_4Ta_{12}\}$ clusters. *J. Mater. Chem. A* **2017**, *5*, 22970–22974.
[64] Li, S. J.; Zhou, Y. F.; Peng, Q. P.; Wang, R. Y.; Feng, X. G.; Liu, S. X.; Ma, X. M.; Ma, N. N.; Zhang, J.; Chang, Y. et al. Controllable synthesis and catalytic performance of nanocrystals of rare-earth-polyoxometalates. *Inorg. Chem.* **2018**, *57*, 6624–6631.
[65] Li, S. J.; Li, G.; Ji, P. P.; Zhang, J. W.; Liu, S. X.; Zhang, J.; Chen, X. N. A giant Mo/Ta/W ternary mixed-addenda polyoxometalate with efficient photocatalytic activity for primary amine coupling. *ACS Appl. Mater. Interfaces* **2019**, *11*, 43287–43293.

Yuan Guan is currently pursuing his master's degree in inorganic chemistry under the supervision of Prof. Xin-Xiong Li at Fuzhou University, China. His main research interests are related to the design, synthesis and application of novel polyoxotantalates.

Xin-Xiong Li received his B.S. (2007) from Fujian Normal University. He then joined Fujian Institute of Research on the Structures of Matter, Chinese Academy of Sciences, where he received his Ph.D. under the supervision of Prof. Guo-Yu Yang in 2012. After that, he worked as a research assistant in the institute and was promoted as an associate professor at December, 2014. Since 2015, he has been working as an associate professor in the College of Chemistry at Fuzhou University. From 2018 to 2019, he worked as a postdoctoral fellow with Prof. Qichun Zhang at School of Materials Science and Engineering, Nanyang Technological University. He worked as a full professor of chemistry in the College of Chemistry at Fuzhou University since September, 2020. His current research interest is focused on the design and syntheses of novel POM clusters and POM-based frameworks with various functions.

Shou-Tian Zheng was born in Fujian, China (1978). He received his B.S. (2001) from Xiamen University. He then joined the Fujian Institute of Research on the Structures of Matter, Chinese Academy of Sciences, where he received his M.S. and Ph.D. under the supervision of Prof. Guo-Yu Yang in 2006 and 2009, respectively. From 2009 to 2013, he joined Prof. Xianhui Bu's group and worked as a postdoctoral fellow on the synthesis and properties of zeolite-type metal-organic frameworks at the California State University, Long Beach. Since 2013, he has been a chemistry professor at School of Chemistry, Fuzhou University, China. His current research interest is focused on the synthesis and properties of giant polyoxometalate macromolecules.